AIAA JOURNAL
Vol. 47, No. 11, November 2009

Flow-Induced Vibrations of Pressure/Temperature Sensors

Karen M. L. Scott,* Thomas D. McQuigg,† Sameer B. Mulani,‡ Rakesh K. Kapania,§ and Joseph A. Schetz¶
Virginia Polytechnic Institute and State University, Blacksburg, Virginia 24060

DOI: 10.2514/1.45016

Flow-induced vibrations of sensors are traditionally predicted through use of the American Society of Mechanical Engineers Boiler and Pressure Vessel Code Section III Appendix N-1300. For an Euler–Bernoulli beam, this code provides engineers with a dynamic response prediction for a given sensor–fluid environment. Engineers can use this information to estimate fatigue life of a particular probe design. However, this tool provides no estimation of shear stresses experienced by the sensor under fluid-structure interaction and can give very conservative results in some cases. Because shear stresses are significant, especially for a low aspect ratio, minimally intrusive sensors or those which vibrate with very high frequencies, shear stresses must be included in the response prediction method. This can be achieved by moving away from Euler–Bernoulli to Timoshenko beam models. Upon making this step, American Society of Mechanical Engineers guidelines must be modified to allow inclusion of shear stresses. A modification to the code is presented which includes not only shear stresses experienced by the sensor, but also the mean response. The use of elliptical sections in preference to circular sections is also explored.

Nomenclature

A = area of cross section, m^2
A_L = lift amplification factor
C_D = mean drag coefficient
C'_D = fluctuating drag coefficient
C'_L = fluctuating lift coefficient
C_n = reduced damping coefficient
C_R = turbulent forcing coefficient
E = modulus of elasticity, Pa
f_s = vortex shedding frequency, Hz
G = shear modulus, Pa
G_f = single-sided power spectral density, $(N/m)^2/Hz$
I = moment of inertia, m^4
J_{nn} = joint acceptance
L_e = correlation length, m
M_n = generalized mass
m_t = total mass per unit length, kg/m
S_t = Strouhal number
S_y = joint acceptance
y_n = displacement amplitude of nth mode, m
α = slope due to bending
β = slope due to shear deformation
ξ_n = modal damping coefficient
ρ = density, kg/m^3
Φ = normalized power spectral density
ϕ_n = nth mode shape
ω_n = natural frequency of vibration, rad^{-1}

Received 17 April 2009; revision received 8 June 2009; accepted for publication 19 June 2009.

*College of Engineering Graduate Teaching Fellow, Department of Aerospace and Ocean Engineering, 215 Randolph Hall. Student Member AIAA.
†Graduate Research Assistant, Department of Aerospace and Ocean Engineering, 215 Randolph Hall. Student Member AIAA.
‡Postdoctoral Associate, Department of Aerospace and Ocean Engineering, 215 Randolph Hall. Member AIAA.
§Mitchell Professor, Department of Aerospace and Ocean Engineering, 215 Randolph Hall. Associate Fellow AIAA.
¶Durham Chair in Aerospace and Ocean Engineering, Department of Aerospace and Ocean Engineering, 215 Randolph Hall. Fellow AIAA.

I. Introduction

FLUID structure interactions, in particular, the vibration of a circular cylinder in a fluid flow, have been investigated for more than a century [1]. In recent times, attempts have been made to introduce design guidelines for engineers, most notably in the American Society of Mechanical Engineers (ASME) Boiler and Pressure Vessel Code (N-1300) [2]. The subject gained particular attention as a result of a sodium leakage incident at a fast breeder reactor, Monju in 1995, caused by high cycle fatigue of a thermometer well subject to flow-induced vibration. Many studies followed [3–6], primarily in Japan, to attempt to improve and validate the analysis methods cited in ASME N-1300. The analysis method presented by ASME requires knowledge of the structural natural frequencies and mode shapes. These natural frequencies and mode shapes are primarily generated using exact solutions of Euler–Bernoulli (EB) beam theory. As is well known, this theory neglects both the shearing of a beam's cross section and the contribution of rotatory inertia. The ASME code applies only to beams for which the length is significantly greater than its depth, usually a 10:1 ratio. Existing sensor designs tend to satisfy this requirement such that Euler–Bernoulli beam theory can be used in the generation of response prediction data with the ASME codes. However, such sensors as studied previously [3–6] have the disadvantage that they are somewhat slender which is not an ideal characteristic when considering fatigue life. Fatigue failure is undesirable as more often than not the broken sensor can contribute to significant foreign object damage, which can lead to significant environmental issues such as that experienced at Monju. The problem has been experienced extensively in cryogenic applications where foreign object damage leads to rocket failure. With these considerations in mind it is advantageous to design a sensor that is minimally intrusive to an internal flow for which the fatigue life is extended while maintaining adequate measurement characteristics. ASME also neglects the startup and shutdown effects through their selection of turbulence model. Although the complete study is beyond the scope of one paper, the first step is the improvement of the analysis tools to deal with less slender, lower aspect ratio sensors in addition to sensors with a noncircular cross section. Shortening the sensor means that shear and rotatory inertia effects now become very important and results generated via integration of the EB theory with ASME guidelines [2] are less reliable for predictions. The mechanism through which the analysis can be improved is through use of the Timoshenko beam theory which is implemented through an energy methods approach. Using this modification, the response prediction can be decomposed into bending and shear stress contributions and

as the sensor aspect ratio decreases it is observed that shear stress contributions become significant. Most sensors are circular in cross section; however, it can be beneficial to consider elliptical cross sections because both the mean and amplitude of the sensor response may be reduced due to a more streamlined shape. Reducing the stresses ultimately leads to extended fatigue life of such a sensor when compared with that with a circular cross section.

II. Euler–Bernoulli vs Timoshenko Beam Theory

A. Euler–Bernoulli Beam Theory

The Euler–Bernoulli beam theory has been in existence since the late 1700s and its use became widespread in large scale applications with the building of the Eiffel Tower and Ferris Wheel [7]. The primary assumption of the theory states that for a slender beam (for which the length:depth ratio is no less than 10:1), shear deformation effects and rotatory inertia can be neglected and thus these drop out from the governing equation of vibration. Thus, the equation for transverse free vibration of an Euler–Bernoulli beam is

$$\frac{\partial^2}{\partial x^2}\left(EI\frac{\partial^2 w}{\partial x^2}\right)+\rho_s A\frac{\partial^2 w}{\partial t^2}=0 \tag{1}$$

where w is the transverse displacement of the beam and x varies along the length of the beam from 0 to L. Equation (1) can be simplified further if a beam of constant cross section is assumed. For simple boundary conditions, an exact solution can be obtained through the assumption of harmonic motion of the beam and application of appropriate boundary conditions. The boundary conditions for a cantilevered Euler–Bernoulli beam which will be used in this study are well known as $w = w' = 0$ at $x = 0$ and $w'' = w''' = 0$ at $x = L$.

Although Euler–Bernoulli beam models are useful in many vibration applications, they are not without limitation. Typically, as the ratio of length to depth drops below 10:1, vibration amplitudes calculated using Euler–Bernoulli beam models start to show deviation from experimental results as the inertial and shear effects become significant. It should be noted that for high aspect ratio beams, where the Euler–Bernoulli model is favored due to its simplicity, shear and inertial effects cannot be ignored for the case of high frequency vibrations. In both this case and that of a lower aspect ratio beam, it is often favored to apply the Timoshenko beam model.

B. Timoshenko Beam Theory

The Timoshenko beam theory includes both rotatory inertia and shear effects. Here, if the total response of the beam is defined as w, then the total slope can be seen to be made up of both a bending (α) and a shear (β) contribution. Derivation of the equations of motion, setting $\beta = \alpha - w'$, then leads to the following two partial differential equations [8]:

$$\begin{aligned}&\frac{\partial}{\partial x}\left[\kappa GA\left(\alpha-\frac{\partial w}{\partial x}\right)\right]+\rho A\frac{\partial^2 w}{\partial t^2}=0\\&\kappa GA\left(\alpha-\frac{\partial w}{\partial x}\right)-\frac{\partial}{\partial x}\left(EI\frac{\partial \alpha}{\partial x}\right)+\rho I\frac{\partial^2 \alpha}{\partial t^2}=0\end{aligned} \tag{2}$$

In this case, the boundary conditions for a cantilevered beam are $w = \alpha = 0$ at $x = 0$ and $\alpha' = \beta = 0$ at $x = L$. Both Eqs. (1) and (2) can be solved using a variety of methods and exact solutions can be obtained for simple boundary conditions [8]. However, it is often not convenient to rely upon and hard code an exact solution because computation with nonideal boundary conditions may be favored in the future. For this reason, it is desirable to write expressions for both the kinetic and strain energies of the system, as these are easily modified for alternate configurations, and solve the system through the use of an approximate method.

C. Eigensolution via Rayleigh–Ritz

The Rayleigh–Ritz method assumes a solution to the system in the form of a linear combination of kinematically admissible trial functions [9]. For the Timoshenko case, the solution approximates both the transverse deflection and rotation and takes the form:

$$w^{(n)}(x,t)=\sum_{i=1}^{n} a_i(t)\Phi_i(x) \tag{3}$$

$$\alpha^{(n)}(x,t)=\sum_{i=1}^{n} b_i(t)\Psi_i(x) \tag{4}$$

a_i and b_i can be further broken down such that $a_i = C_i e^{j\omega_n t}$ and $b_i = D_i e^{j\omega_n t}$ (assuming a harmonic beam response for free undamped vibration). Using this, we substitute Eqs. (3) and (4) into the beam energy expressions, minimize the function, and thus generate the classic eigenvalue problem (see Meirovitch [9]):

$$|\mathbf{K}-\omega^2\mathbf{M}|=0 \tag{5}$$

Solving this problem for n trial functions for both w and α leads to the generation of $2n$ eigenvalues (ω^2) and $2n$ eigenvectors for which the components correspond to $C_i^{(n)}$ and $D_i^{(n)}$. Selection of trial functions Φ and Ψ depends on the boundary conditions for the problem at hand, though it is imperative that the functions form a complete set. It is necessary to only satisfy the essential boundary conditions, though violation of the natural boundary conditions will lead to slow convergence. With suitable trial functions in place, the system can often be solved producing excellent results with only a few trial functions [9]. This is particularly advantageous if wishing to design a control system to limit vibration.

For circular cross sections, the differential equations for transverse displacements in both the Euler–Bernoulli and Timoshenko beam theories are independent of x and y directions. Mode shapes and eigenvalues are identical in each of these transverse directions due to identical mass moments of inertia. Hence, the torsional differential equation can be decoupled so warping does not occur. This simplification makes sensors with a circular cross section an obvious choice. However, circular cross sections suffer the disadvantage that they experience increased mean drag and fluctuating drag force as compared with slimmer sections. With this in mind, it may be advantageous to consider elliptical cross sections, which may improve fatigue life. An obvious disadvantage is during manufacture of noncircular sections, it may be more likely for asymmetry to form in the structure which now means that a set of coupled equations needs to be considered. Information regarding flexural–torsional coupling with Timoshenko's beam theory may be found in [10].

III. Fluid-Structure Interaction Analysis Tools

Regardless of the method used to solve the beam vibration problem, natural frequencies and mode shapes of the beam can be obtained. These frequencies and mode shapes feed into the design code for flow-induced vibrations which is specified by the ASME Boiler and Pressure Vessel Code Section III Division I Appendix N-1300 [2]. The code comprises two main areas of analysis: vortex induced vibration and turbulence induced vibration. Using the methods outlined in this code, engineers can quickly obtain information regarding the response amplitude of a sensor in a given fluid flow. Using this information, the mean and rms stresses calculated by the code can be used in a fatigue analysis.

A. Vortex Shedding

Vortices are shed from an inline sensor periodically, hence giving rise to an alternating lift force which is representative of a deterministic system. The frequency of this lift force is the vortex shedding frequency $f_s = S_t U/D$, where S_t is the Strouhal number, a dimensionless parameter used to characterize oscillatory flow. The oscillating lift force can be expressed as

$$F = C_L' JqDL[\sin(2\pi f_s t)] \tag{6}$$

where C_L' is the oscillating lift coefficient, J is the correlation coefficient, q is the dynamic pressure, U is the average freestream

velocity, D is the cylinder diameter, and L is the cylinder length. C'_L, f_s, and J are all functions of Reynolds number [2] and are usually determined experimentally. Often, a conservative value of 1 for C'_L and J is chosen though this assumes the flow is fully correlated over the entire cylinder length. In fact, the correlation length (L_e) for stationary cylinders is often around 3–7 diameters (where $J^2 = L_e/L$). However, caution should be used as Eq. (6) is only valid for the off-resonance condition. Several checks exist to determine if resonance (lock-in) can be avoided [2]:

1) Lift and drag direction lock-in are avoided if the reduced velocity for the fundamental vibration satisfies $U/f_1D < 1$, where f_1 represents the fundamental natural frequency (Hz) of vibration of the structure.

2) Reduced damping for an nth individual mode is large enough ($C_n > 64$) where C_n is

$$C_n = \frac{4\pi\xi_n M_n}{\rho D^2 \int_{Le} \phi_n^2(x)\mathrm{d}x} \tag{7}$$

where ξ_n is the modal damping coefficient, M_n is the generalized mass, ρ is the fluid density, and L_e is the length of the region of the cylinder assumed to be subject to lock-in crossflow (approximately 3-D [6]).

3) For a given vibration mode $U/f_nD < 3.3$ and $C_n > 1.2$, where f_n is the nth natural frequency of vibration.

However, in many industrial applications, lock-in synchronization cannot be avoided. In this case, the vortex induced response must be calculated. The ASME code uses a derivation by Blevins [11], which shows that the maximum displacement (y_n^*) for a particular mode is

$$\frac{y_n^*}{D} = \frac{C_L J \phi_n^*}{16\pi^2 S_t^2 [m_t \xi_n/(\rho D^2)]} \tag{8}$$

where ϕ_n^* is the maximum value of the nth mode shape. This model assumes a uniform structure and a uniform flowfield. This and subsequent models require that the modes be normalized such that the maximum value of a particular eigenvector is 1. An updated version of this equation, which gives displacement in the lift direction for the nth mode ($y_{L,n}$) as a function of position and allows for varying sensor diameter, $D(x)$, is [12]

$$y_{L,n}(x) = \frac{\rho V^2 C'_L \int_{Le} D(x)\phi_n(x)\,\mathrm{d}x}{2(2\pi f_n)^2 \int_0^L m_t(x)\phi_n^2(x)\,\mathrm{d}x} A_L \phi_n(x) \tag{9}$$

where the lift amplification factor A_L is defined as

$$A_L = \frac{1}{\sqrt{\{1 - (\frac{f_s}{f_n})^2\}^2 + \{2(\xi_n + \zeta_n)\frac{f_s}{f_n}\}^2}} \tag{10}$$

Modal fluid damping ζ_n is

$$\zeta_n = \frac{1}{4}\left(\rho D^2 \int_{Le} \phi_n^2(x)\,\mathrm{d}x\right)\left(\frac{U}{2\pi f_n D}\right) \tag{11}$$

and m_t is the total cylinder mass per unit length which includes displaced fluid mass. The physical displacement of the sensor is then simply obtained by the principle of modal superposition.

Equations (9) and (10) can easily be modified for fluctuations in the drag direction by replacing subscript L with D and f_s with $2f_s$ [12]. Blevins [11] suggested that C'_L and C'_D have values of 0.6 and 0.06, respectively. A value of 0.6 for the lift coefficient is somewhat conservative; hence if this value is used in our calculations the correlation with experimental values will be poor. Because it is known that a fluctuating lift coefficient is a function of a displacement amplitude, it is possible to use an iterative scheme, by using an estimate of C'_L to start iterative procedures, to compare the calculated displacement amplitude with that given in a displacement amplitude versus fluctuating lift coefficient chart provided by Blevins [11]. One must note, however, that these equations and the iterative scheme which was implemented are limited in that they can only be used up to the point of resonance. In the lock-in region, prediction of response is possible using the full nonlinear model as given by Blevins [11], but many experimental coefficients must be obtained to adjust the model for the particular vortex induced vibration environment being studied.

B. Turbulence Model

The ASME guidelines [2] present an analysis method to predict vibratory response of a sensor due to turbulence.

The development of this response equation stems from the simple relation for standard deviation (assuming a zero-mean response):

$$y^2(x) = \int_{-\infty}^{\infty} S_y(x,\omega)\,\mathrm{d}\omega \tag{12}$$

$S_y(x,\omega)$ is the power spectral density of the displacement due to a random pressure fluctuation and varies with power spectral density of the pressure (S_p) which is assumed to be stationary in nature. However, the expression for $S_y(x,\omega)$ remains rather complicated. To simplify the expression, the following assumptions are used (see [13,14] for details).

1) Cross terms are negligible in the transfer function.

2) Turbulence is homogeneous; this is usually not true in real life but it is a necessary simplifying step.

3) The acceptance integral is a slowly varying function of ω close to the natural frequency, but this is usually only valid for systems with damping of 5% or less.

Au-Yang [13,14] showed that Eq. (12) becomes (for these restrictions)

$$y^2(x) = \sum_n \frac{LG_f(f_n)\phi_n^2(x)}{64\pi^3 M_n^2 f_n^3 \xi_n} J_{nn} \tag{13}$$

Here the single-sided power spectral density $G(f)$ is

$$G_f(f_n) = \Phi(f_n)\left(\frac{1}{2}\rho U^2 D\right)^2\left(\frac{D}{U}\right) \tag{14}$$

where the normalized power spectral density $\Phi(f)$ is

$$\Phi(f_n) = \frac{4C_R^2}{1 + (2\pi f_n D/U)^2} \tag{15}$$

and J_{nn} and C_R are defined as joint acceptance integral and turbulent forcing coefficients, respectively. J_{nn} can be quite a complex expression and hence the upper bound of 1 is often taken in calculations [13]. However, special cases for crossflow over beams exist. The most widely accepted approximation is

$$J \approx 2L_e/L \tag{16}$$

which is valid up to $L_e/L \approx 0.06$ [14] for beams with arbitrary boundary conditions. Insensitivity to beam boundary conditions is explained by Au-Yang in [14] by the definition of joint acceptance: "a measure of the integrated effect over the surface of the structure," which is therefore "not very sensitive to local changes in the slopes of the mode shapes due to differences in the boundary conditions." Justification for use of Eq. (16) for flow-induced vibration of beams is given by both Blevins [11] and Au-Yang [14] and both recommend the correlation length L_e to be between 3 and 5 diameters. The validity of this approximation comes into question for shorter beams and is thus something which will have to be further explored following this initial study.

Although Eq. (13) has been proven by many authors throughout the last 30 years, few have offered expansion or modification of the expression to help with applicability to real world problems. Dozaki et al. [12] presented a slight modification to this formulation, Eq. (17), which included the contribution of fluid damping. Although this is somewhat limited in applications involving air, it is very important to include this effect for structures vibrating in fluids such as water:

$$y(x) = \sum_n \sqrt{\frac{L_e G_f(f_n) J_{nn} \int_{L_e} \phi_n^2(x)\mathrm{d}x}{64\pi^3 M_n^2 f_n^3(\xi_n + \zeta_n)}}\phi_n \tag{17}$$

C. Implementation and Extraction of Shear Stresses

To successfully use the presented formulations the mode shapes of a freely vibrating structure are required. It is possible to insert the results for approximate mode shapes for w only into these equations and obtain, through extraction, the contribution of shear to the sensor's response. To approximate this, a constant distributed load is applied to the beam to be analyzed. For this we use the approximate mean drag coefficient experienced by the sensor (determined empirically as a function of the Reynolds number) and a boundary-layer approximation to give a distribution profile for force. With this forcing and application of the Ritz method, the coupled bending and shear expressions are solved and hence for each point along the beam, the percentage contribution of shear is known. This percentage contribution is applied to the results determined from the preceding analysis; hence, mean and rms shear stresses can be obtained. A derivation of the variance of the shear stresses σ_{zx} as a function of the variance of the axial stress (bending), σ_{xx} for a beam.

Axial stress σ_{xx} and shear stress σ_{zx} in the beam using the Timoshenko theory are given by Eqs. (18) and (19), respectively,

$$\sigma_{xx} = -Ez\frac{\partial\alpha}{\partial x} \tag{18}$$

$$\sigma_{zx} = kG\left(\frac{\partial w}{\partial x} - \alpha\right) \tag{19}$$

where E and G are elastic modulus and shear modulus, respectively; α is the rotation caused by the bending only, and w is the transverse displacement of the beam. The ratio of bending stress, σ_{xx}, and shear stress, σ_{xz}, is defined as follows:

$$\frac{\sigma_{xx}}{\sigma_{zx}} = \frac{-Ez\frac{\partial\alpha}{\partial x}}{kG(\frac{\partial w}{\partial x} - \alpha)} \tag{20}$$

While solving for dynamic response or the eigenvalue problem using the Rayleigh–Ritz method, w and α are approximated by trial functions given in Eqs. (3) and (4).

If we substitute these trial functions into Eq. (20), we get

$$\frac{\sigma_{xx}}{\sigma_{zx}} = \frac{-Ez}{kG}\frac{[\sum_{i=1}^{m} b_i\Psi_i'(x)]}{[\sum_{i=1}^{n} a_i\Phi_i'(x) - \sum_{i=1}^{m} b_i\Psi_i(x)]} \tag{21}$$

In Eq. (21), time dependability of the coefficients is not represented for the compact representation of the equation. At the particular height,$z = z_0$, and the location along the beam, $x = x_0$, we get a ratio of σ_{xx} and σ_{zx} as a constant if $\Phi_i(x)$ and $\Psi_i(x)$ are functions of x only. Hence for a particular x, y, and z location:

$$\frac{\sigma_{xx}}{\sigma_{zx}} = C_0 \tag{22}$$

Table 1 Probe sizing and material properties

Property	Symbol	Value
Elastic modulus	E	1.5 GPa
Density	ρ_p	1240.0 1240.0 kg/m^3
Mass per unit length	m_p	0.0279 0.0297 kg/m
Outer diameter	OD	6.223 mm
Inner diameter	ID	3.175 mm
Moment of inertia	I	6.859×10^{-11} m^4
Length	L	38.1 mm

Therefore, variance of the shear stress is given as follows:

$$\mathrm{Var}\,(\sigma_{zx}) = \sigma_{xx}/C_0^2 \tag{23}$$

IV. Experimental Validation

Experimental validation of the analytic models took place in the Baker Hydraulics Laboratory of the Civil and Environmental Engineering Department at Virginia Polytechnic Institute and State University. The Hydraulics Lab is home to three sediment demonstration channels for which the primary purpose is to study water body sedimentation and associated water flow. The smallest of the three channels, a 20 ft Engineering Laboratory Design, Inc., Sediment Demonstration Channel, was used here.

A. Test Apparatus and Materials

From a holding tank, two gravity-fed hydraulic pumps send water through a system of polyvinyl chloride (PVC) pipes to the channel head, where they then run back to the holding tank. Water from the two pumps combines after a short distance. The water can then be sent either through a 2 in. pipe or a 6 in. pipe or both, depending on the capacity requirements of the current test. This arrangement is controlled by the appropriate ball valves. One or two pumps may be used; however, the second pump is only used if the larger pipe is used. Volumetric flow rate can be monitored using the appropriate Venturi nozzles and the corresponding supplied water and mercury manometers.

The original channel was modified for this experiment by replacing a section of the 2 in. pipe running underneath the channel with an experimental test section. The original section of white PVC was replaced by an identical section of clear PVC. An aluminum bossing was then constructed for the purpose of supplying a mounting location for the faux temperature sensor to be studied. For this experiment only the first hydraulic pump was used, and flow only traveled through the 2-in.-diam test section piping.

Because fluid flow through the channel would not have provided enough fluid force on a typical AISI 304 stainless steel sensor, an alternate material was used. Low-damping PVC was chosen as the replacement for the faux sensor for which the material and geometric properties can be found in Table 1. Figure 1a shows the probe in a housing.

To mount the PVC tube in the test section, it was fitted with an aluminum bushing attached with silicone. Then, a brass Swagelok fitting with nylon inserts was used to secure the bushing inside of the

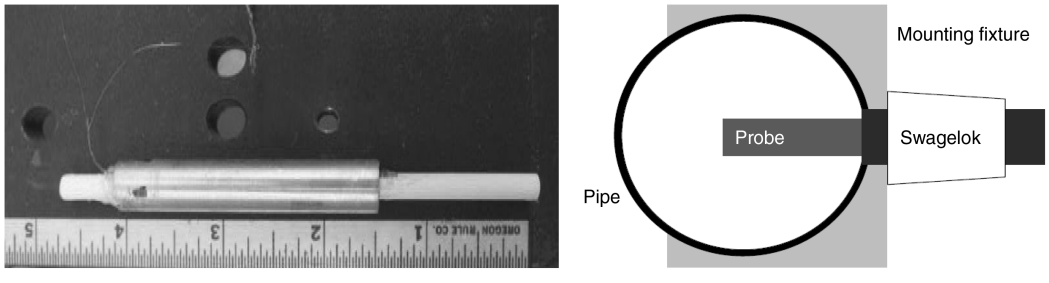

a) b)

Fig. 1 Shown are the following: a) PVC probe in aluminum bushing, and b) illustration of installation.

bossing. This configuration produced a secure, undamaged PVC probe when mounted in the test section (see Fig. 1b, not to scale).

B. Measurement and Data Capture

Strain data were recorded using foil Vishay strain gauges mounted at the fixed end of the beam where the bending strain is a maximum. A single gauge was used with wiring in a quarter Wheatstone bridge circuit. Data were collected for both lift and drag direction responses by rotating the mounted probe to the appropriate orientation. A sample probe is shown in Fig. 1a. Analog voltage data were amplified using a Micromeasurements 2310 Signal Conditioning Amplifier. A Tektronix TDS 2014 digital oscilloscope was then used to collect and store all data. Data processing and analysis was performed using MATLAB version 2008b. To reduce noise recorded, all electronic measurement equipment was connected to a ground isolating transformer. In addition, both channel vibrations interfering with data collection of the probe vibration, as well as water temperature fluctuation effect on strain gauge readings were considered. However, both were found to have minimal effect on the recorded data.

Flow data were captured using the water channel's attached mercury and water manometers. Manometer measurements are related to pump frequency but variations in the water tank head require a calibration to be performed before each test.

C. Data Analysis

Data analysis was performed to find an experimental correlation between flow velocity and measured strain, as well as the probe's natural frequency. For a given data point 2500 samples were collected over a 1 s interval. The average of the strain recorded at each sample was calculated, as well as the standard deviation. For a set of data, the average and rms response was plotted versus flow velocity and compared with the results predicted by analysis. In addition, data were converted from the time domain to the frequency domain to determine the measured probe natural frequency of the probe. This was compared with that predicted by Timoshenko's beam theory which considers not only the probe but also the added mass effect and showed excellent agreement.

V. Results

A. Comparison with Experimental Data

Observations during the course of experimentation have resulted in a progressive cycle of experimentation, analysis, and refinement of experimental procedures and equipment. Experimental results have shown successful data capture and seem to fit the analytical model quite well for mean and rms strains as shown in Figs. 2a, 2b, and 3. The largest discrepancies are seen for the lower velocities. Because we are dealing with such low velocities and much lower strains, experimental errors in this region are amplified. In addition, the prediction model used is known to have problems for low amplitudes of vibration seen at these lower velocities [11].

The same analysis predicts the shear stresses experienced by the probe (Figs. 4a and 4b). In these plots, the experimental values obtained by experiment for bending strains have been treated by the method described in Eqs. (19–23) to give so-called extracted shear strains to aid comparison in the plot.

To ensure the analysis method is still compatible with longer, slender probes a comparison case with Kawamura et al.'s results was generated for displacement amplitudes [15]. As before, the results show good agreement, except at lower reduced velocities (see Fig. 5), which is again a known weakness of the model. Shear strains are also predicted (not shown) which are at maximum 100 $\mu\epsilon$.

B. Potential of Elliptical Sensor Sections

It was noted earlier that substantial benefit may be obtained from having sensors using elliptical sections (with major diameter aligned with flow direction) in preference to circular sections. Figure 6 illustrates the reduced frontal area when considering an elliptical section with a major/minor axis ratio of 2, keeping the characteristic length constant. Not only should the mean drag coefficient be reduced, but the fluctuating lift and drag coefficients also. It follows that the overall response in the drag direction should be substantially reduced. However, response amplitude in the lift direction may in fact increase due to the slender nature of the sensor in this direction. Delany and Sorensen [16] indicate that the mean drag coefficient for an ellipse with a major to minor axis ratio of 2 is approximately 60% of that for a circular cylinder. This approximation was later used by Li et al. in [17] and confirmed during their numerical study. Investigations by Modi and Wiland [18] and Kim [19] suggest that the fluctuating coefficients also reduce to less than 60% of the circular cylinder values. However, 60% will be used to be conservative. Using these approximations, a simulation was performed for an

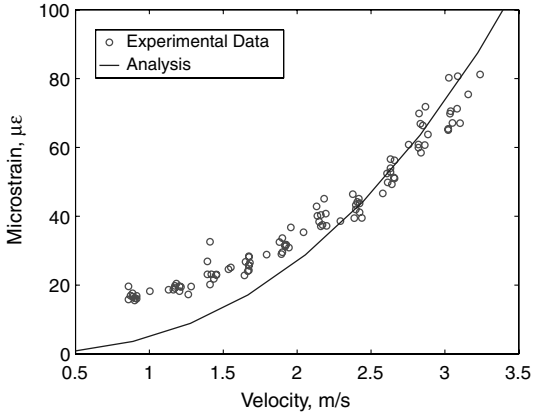

a) Normal strains in drag direction

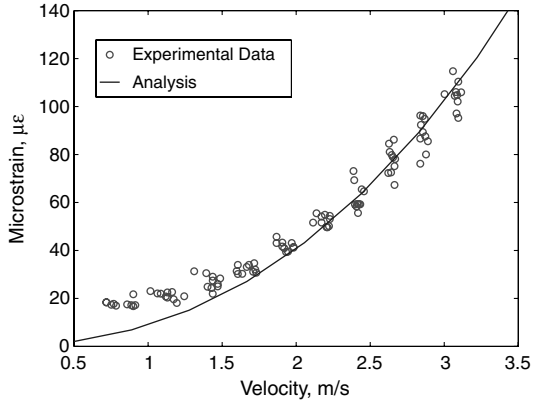

b) Normal strains in lift direction

Fig. 2 Comparison of variation of rms strains with tests in water flume for circular cross section.

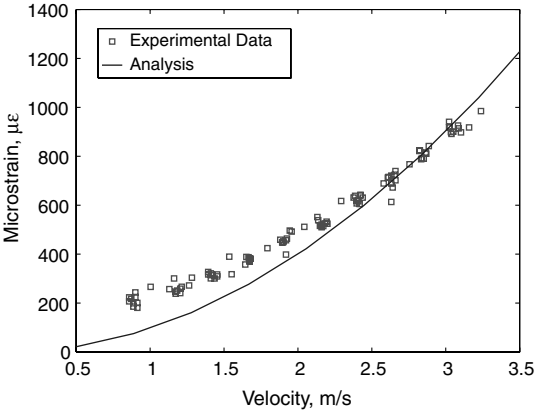

Fig. 3 Comparison of variation of mean strains with tests in water flume for circular cross section.

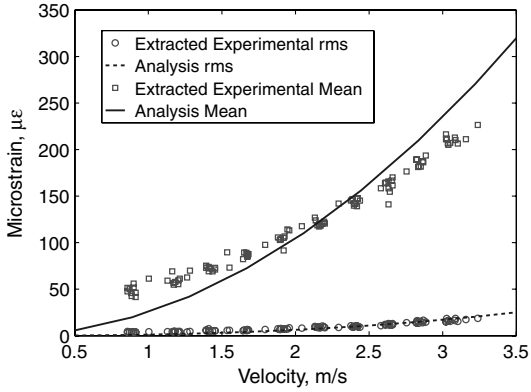

a) Mean and rms shear strains in drag direction

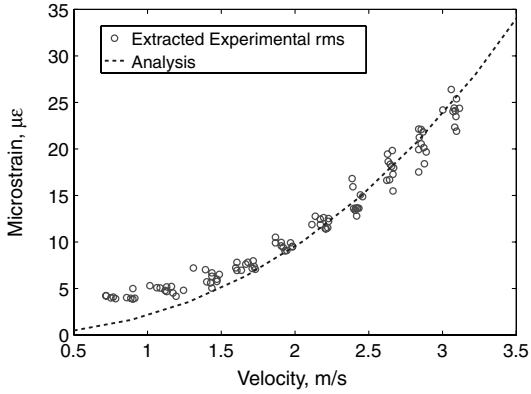

b) RMS shear strains in lift direction

Fig. 4 Predicted shear strains for circular cross section.

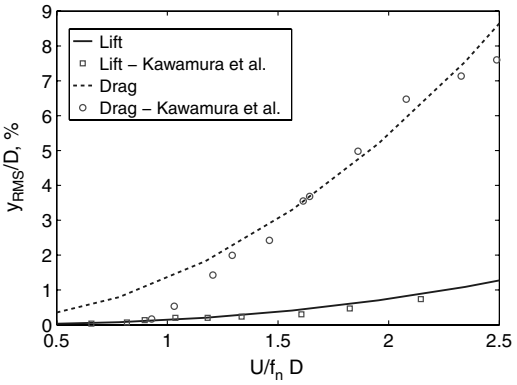

Fig. 5 Comparison of predicted amplitudes with Kawamura results for length:diameter ratio ≈ 10 [15].

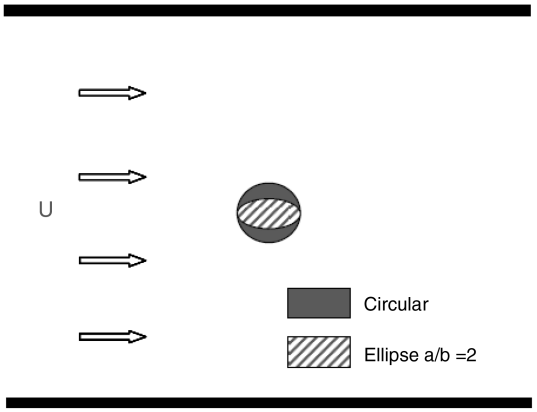

Fig. 6 Illustrating the reduced frontal area of an elliptical cross section.

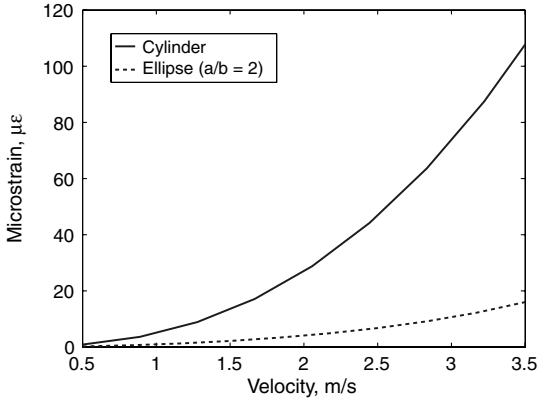

a) RMS strains in drag direction

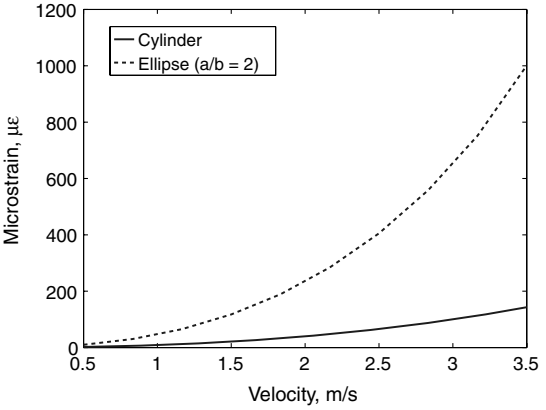

b) RMS strains in lift direction

Fig. 7 Comparison of fluctuating response of elliptical and circular sections for experimental conditions.

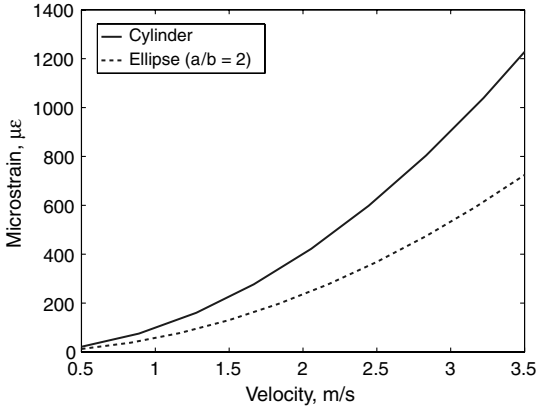

Fig. 8 Comparison of mean response of elliptical and circular sections for experimental conditions.

elliptic cylinder with major/minor axis ratio of 2 with the same flow conditions and material properties as for the circular cylinder described in the previous section.

A significant reduction in both mean and rms drag strains is shown by Figs. 7a, 8, 9a, and 10. However, lift rms strains are increased significantly as shown in Figs. 7b and 9b. This shows that perhaps a ratio of 2 is somewhat ambitious and a lower ratio would be better suited to this problem. Selection of the ideal ratio leads to an optimization problem which will be attempted in the future.

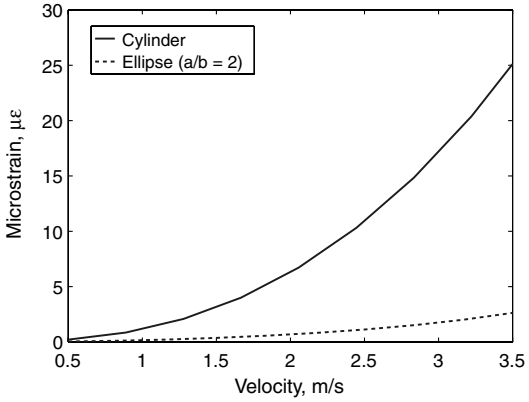

a) RMS shear strains in drag direction

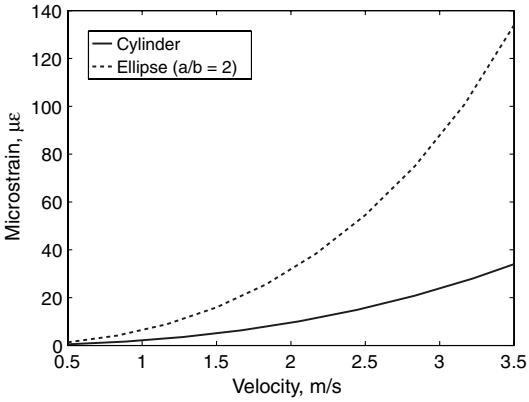

b) RMS shear strains in lift direction

Fig. 9 Comparison of fluctuating shear response of elliptical and circular sections for experimental conditions.

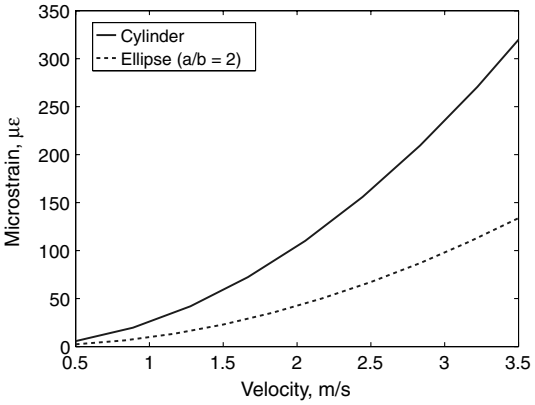

Fig. 10 Comparison of mean shear response of elliptical and circular sections for experimental conditions.

VI. Conclusions

The ASME recommendations for sensor design are updated to include shear deformation of the sensor. Bending strains in the lift and drag directions were experimentally validated using water flow at a range of velocities. Suitability of elliptical cross-sectional sensors over circular sensors is shown, though an optimal solution was not calculated at this point. Currently the mean drag coefficient, the fluctuating drag coefficient, and the fluctuating lift coefficient for an elliptical section are taken from literature. To explore further major/minor axis ratios, a return to literature followed by a switch to numerical computations will be required. Reducing the principal stresses which inherently lead to fatigue failure of such sensors is an optimization problem where the major/minor axis ratio is optimized for a given flow condition. Regardless of sensor cross section, it is more than often the case that the sensors are manufactured from solid stock. The central hole placements for wires, etc., as well as the size of the hole are uncertainties as a discrepancy between flexural and shear axis may exist. Including these uncertainties is an important next step for elliptical cross sections as a small uncertainty in the angle of attack (from mounting) can lead to major stresses in the principal stresses. The design of elliptical cross-sectional sensors is therefore best suited to a reliability based design optimization.

Acknowledgments

The authors would like to thank Mark Montgomery, Bruce Stanger, and all staff of the Baker Hydraulics Laboratory for their assistance with the experimental portion of this work. Finally, the authors would like to thank Vladimir Kochergin and Matt Palmer of Luna Innovations for their support.

References

[1] Kawamura, T., Nakao, T., Hayashi, M., and Gotoh, N., "Experimental Studies on Vibrations of a Circular Cylinder in Cross Flow at Supercritical Reynolds Numbers," *American Society of Mechanical Engineers, Pressure Vessels and Piping Division (Publication) PVP*, Vol. 363, American Society of Mechanical Engineers, Fairfield, NJ, 1998, pp. 35–44.

[2] Anon., "Section III Division I," *ASME Boiler and Pressure Vessel Code*, Vol. 1, Oct. 1998, pp. 219–240.

[3] Okajima, A., Kosugi, T., and Nakamura, A., "Experiments on Flow-Induced In-Line Oscillation of a Circular Cylinder in a Water Tunnel (1st Report, The Difference of the Response Characteristics When a Cylinder is Elastically Supported at Both Ends and Cantilevered)," *JSME International Journal, Series B (Fluids and Thermal Engineering)*, Vol. 44, No. 4, 2001, pp. 695–704. doi:10.1299/jsmeb.44.695

[4] Nakamura, A., Okajima, A., and Kosugi, T., "Experiments on Flow-Induced In-Line Oscillation of a Circular Cylinder in a Water Tunnel (2nd Report, Influence of the Aspect Ratio of a Cantilevered Circular Cylinder)," *JSME International Journal, Series B (Fluids and Thermal Engineering)*, Vol. 44, No. 4, 2001, pp. 705–11.

[5] Sakai, T., Iwata, K., Morishita, M., and Kitamura, S., "Vortex-Induced Vibration of a Cantilever Circular Cylinder in Super-Critical Reynolds Number Flow and its Suppression by Structure Damping," *JSME International Journal, Series B (Fluids and Thermal Engineering)*, Vol. 44, No. 4, 2001, pp. 712–720. doi:10.1299/jsmeb.44.712

[6] Iwata, K., Morishita, M., Sakai, T., Yamaguchi, A., and Ogura, K., "Evaluation of Turbulence-Induced Vibration of a Circular Cylinder in Supercritical Reynolds Number Flow," *JSME International Journal, Series B (Fluids and Thermal Engineering)*, Vol. 44, No. 4, 2001, pp. 721–728. doi:10.1299/jsmeb.44.721

[7] Han, S. M., Benaroya, H., and Wei, T., "Dynamics of Transversely Vibrating Beams Using Four Engineering Theories," *Journal of Sound and Vibration*, Vol. 225, No. 5, 1999, pp. 935–988. doi:10.1006/jsvi.1999.2257

[8] Craig, R. R., and Kurdila, A. J., *Fundamentals of Structural Dynamics*, Wiley, New York, 2006, 2nd ed..

[9] Meirovitch, L., *Fundamentals of Vibrations*, McGraw–Hill, New York, 2001, International Edition.

[10] Bercin, A. N., and Tanaka, M., "Coupled Flexural-Torsional Vibrations of Timoshenko Beams," *Journal of Sound and Vibration*, Vol. 207, No. 1, 1997, pp. 47–59. doi:10.1006/jsvi.1997.1110

[11] Blevins, R. D., *Flow-Induced Vibration*, Krieger, Malabar, FL, 1986.

[12] Dozaki, K., Morishita, M., and Iwata, K., "Modification and Design Guide of Thermowell for FBR," *American Society of Mechanical Engineers, Pressure Vessels and Piping Division (Publication) PVP*, Vol. 363, American Society of Mechanical Engineers, Fairfield, NJ, 1998, pp. 125–133.

[13] Au-Yang, M. K., "Joint and Cross Acceptances for Cross-Flow-Induced Vibration—Part 2: Charts and Applications," *Journal of Pressure Vessel Technology*, Vol. 122, No. 3, 2000, pp. 355–361. doi:10.1115/1.556192

[14] Au-Yang, M. K., "Joint and Cross Acceptances for Cross-Flow-Induced Vibration—Part 1: Theoretical and Finite Element Formulations,"

Journal of Pressure Vessel Technology, Vol. 122, No. 3, 2000, pp. 349–354.
doi:10.1115/1.556191

[15] Kawamura, T., Nakao, T., Hayashi, M., and Murayama, K., "Strouhal Number Effect on Synchronized Vibration Range of a Circular Cylinder in Cross Flow," *JSME International Journal, Series B (Fluids and Thermal Engineering)*, Vol. 44, No. 4, 2001, pp. 729–37.

[16] Delany, N., and Sorensen, N., "Low-Speed Drag of Cylinders of Various Shapes," *National Advisory Committee for Aeronautics—Technical Notes*, 1953.

[17] Li, Z., Davidson, J., and Mantell, S., "Numerical Simulation of Flow Field and Heat Transfer of Streamlined Cylinders in Cross Flow," *Transactions of the ASME: Journal of Heat Transfer*, Vol. 128, No. 6, 2006, pp. 564–570.
doi:10.1115/1.2188463

[18] Modi, V. J., and Wiland, E., "Unsteady Aerodynamics of Stationary Elliptic Cylinders in Subcritical Flow," *AIAA Journal*, Vol. 8, No. 10, 1970, pp. 1814–1821.
doi:10.2514/3.5995

[19] Kim, M.-S., "Unsteady Viscous Flow over Elliptic Cylinders at Various Thickness with Different Reynolds Numbers," *17th AIAA Computational Fluid Dynamics Conference*, AIAA, Reston, VA, June 2005.

J. Wei
Associate Editor